JACC Vol. 45, No. 12, 2005
June 21, 2005:1954–60

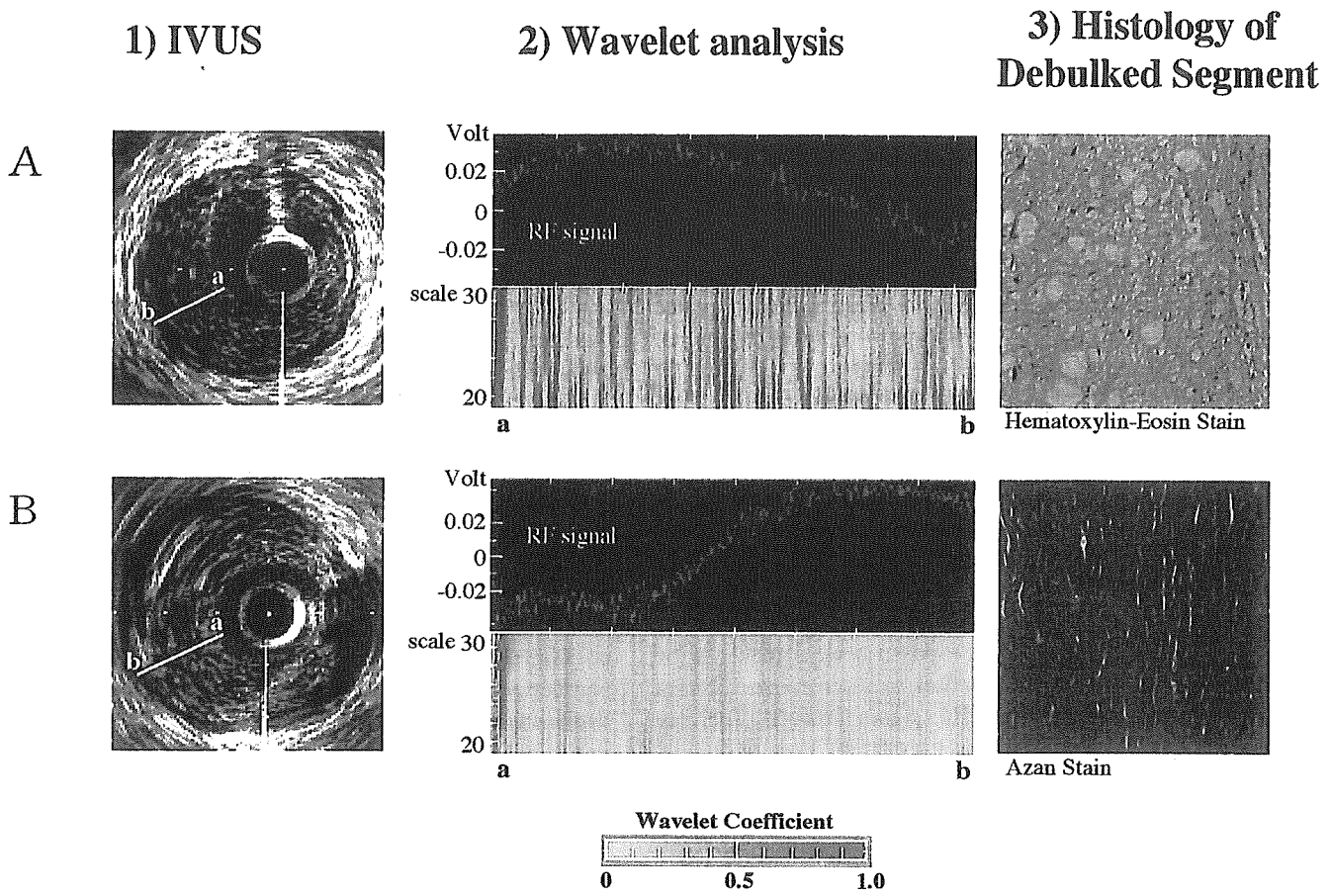

Figure 5. Representative examples of in vivo wavelet analysis of radiofrequency (RF) intravascular ultrasound (IVUS) signals from a lipid-laden plaque **(A)** and from a fibrous plaque without a lipid core **(B)**. The **left panels** show conventional IVUS images, the **middle panels** show the results of wavelet analysis, and the **right panels** show the histologic cross sections of the corresponding directional coronary atherectomy specimen with hematoxylin-eosin and Azan stains. A similar pattern of color mapping was observed from the radiofrequency signal vector of a lipid-laden plaque, as seen in the in vitro study.

pattern as the in vitro results (Fig. 5). Using the same criteria of the wavelet analysis as in the in vitro study, fatty plaque could be detected from the clinical material with a sensitivity of 81% (13 of 16) and a specificity of 85% (11 of 13).

DISCUSSION

The present study is the first report of in vitro as well as in vivo tissue characterization of atherosclerotic plaque using a wavelet analysis of RF IVUS signals. The major finding of this study is that this wavelet method is accurate in detecting lipid-laden atherosclerotic plaque. This method may be useful in assessing plaque vulnerability in patients with coronary artery disease.

Advantages of wavelet analysis. The theoretical basis of wavelet analysis was first developed by Grossmann and Morlet in 1983 (25). Wavelet analysis is a time-frequency domain analysis of signals. The most well known of these is Fourier analysis, which breaks down a signal into constituent sinusoids of different frequencies. The Fourier transform was modified into a transform to analyze only a small section of the signal at a time by looking at "windows" of the signal. This short-time Fourier transform provides some information about when and at what frequencies a signal event occurs. The major drawback of this method is that once a particular size for the time window is chosen, that window is the same for all frequencies. If the window size is changed to a shorter one to increase time (space) resolution, the frequency resolution is compromised. Wavelet analysis was proposed in an attempt to overcome the problems in resolution.

Wavelet analysis represents a windowing technique with variable-sized regions. Wavelet analysis allows the use of long-time intervals when more precise low-frequency information is needed and shorter regions when high-frequency information is needed. One major advantage of wavelets is their ability to analyze a localized area of a larger signal. In this study, the Daubechies-2 wavelet proved best for detecting a lipid-laden plaque. An empirical selection of wavelet has to be made when applying wavelet analysis in a novel field of data. If a new wavelet family is developed, the sensitivity and specificity for detection of fatty tissue may be improved.

Wavelet scales 20 and 30 correspond to wavelengths of 32 and 47 μm, respectively. A scale of <20 is less than conventional IVUS resolution (26) or the ultrasound pulse

wavelength. The results from wavelet analysis with a wavelet scale <20 would measure artificial noise only. A higher value of wavelet correlation coefficient represents an acoustic signal derived from a more complicated structure. Compared with a fibrous area, a fatty area usually is composed of various kinds of tissue, such as lipid-laden foam cells, cholesterol crystals, extracellular lipids, necrotizing material, and fibers, which may be intermingled in a way that could produce complex acoustic impedance mismatches inside the plaque (17). Therefore, a lipid-laden area provides a higher value of wavelet correlation coefficient with a shorter scale of wavelet.

Comparison with other methods of tissue characterization. It was originally expected that tissue components within plaque could be identified from the video-intensity pattern of IVUS images (4,5,7,12–15). Subsequent studies, however, demonstrated significant limitations of tissue characterization by IVUS intensity patterns alone, especially in discriminating fibrous and fatty tissues or in assessing plaque vulnerability (16–19). To overcome the limitations, some authors (20–23) have proposed several methods of quantitative tissue characterization to discriminate fibrous and fatty plaque, including RF signal analysis, such as integrated backscatter analysis, attenuation slope mapping (19,24), and spectral analysis (27). Recently, IVUS elastography was proposed as a novel modality of tissue characterization with IVUS (28). Our laboratory previously reported that color mapping of the angle-dependent echo-intensity was useful for detecting fibrous caps within plaques (29). However, this method has difficulties in detecting other type of tissues. Because none of these previously reported techniques has become available commercially, no study has yet compared their clinical feasibility using the same subjects.

Study limitations. For the in vitro study, the arteries were imaged after they were fixed in formalin at room temperature. It is unknown whether formalin fixation or change in temperature will alter the results of this analysis. Another limitation was the use of nonpressure-distended arteries. When removed from physiologic pressure, atherosclerotic arteries contract. This contraction could significantly alter the architecture, which might affect the wave pattern of the RF IVUS signal. However, the in vivo application of the wavelet analysis also offered similar sensitivity and specificity for identifying a lipid-laden plaque as in the in vitro study. Therefore, these effects appear to be negligible in this study.

This wavelet analysis was performed for one single vector. The single vector analysis is subject to mismatch because of rotation of the images. To minimize any mismatch, we superimposed a radial line from the catheter center onto a conventional cross-sectional IVUS video image to enable the recognition of the location of each vector. In the in vitro study, all the plaques analyzed had a thickness >0.5 mm, and any lipid core had a thickness >0.3 mm. Therefore, we do not know whether it is possible to analyze thinner plaques or to identify very thin lipid cores with this method. Furthermore, the presence of blood and phasic pressure within the lumen as well as any noncoaxial alignment of the catheter may impair appropriate analysis in vivo with this method.

This study was performed on the off-line basis, taking an hour or so to obtain each color map. Therefore, a further development is necessary to be able to provide an on-line plaque evaluation during the study so that immediate feedback is given to the operator.

Conclusions. The present study demonstrates the feasibility of in vitro as well as in vivo tissue characterization by wavelet analysis of RF IVUS signals. Using wavelet analysis, lipid-laden plaque could be detected with a sensitivity and specificity of >80%. This method may be useful in assessing plaque vulnerability in patients with coronary artery disease. Currently, there is no reliable, commercially available device that is capable of discriminating fibrous and fatty areas within atherosclerotic plaque. Detection of vulnerable plaque or sequential observations of the stabilizing effect of lipid-lowering therapy on plaque composition with acceptable accuracy in vivo could improve the management of patients with coronary artery disease. Further evaluation of wavelet analysis in comparison with clinical data and inflammatory markers will be necessary to assess its usefulness in clinical practice to predict future cardiac events in patients with coronary artery disease.

Reprint requests and correspondence: Dr. Takafumi Hiro, Division of Cardiovascular Medicine, The Department of Medical Bioregulation, Yamaguchi University Graduate School of Medicine, 1-1-1 Minami Kogushi, Ube, Yamaguchi 755-8505, Japan. E-mail: thiro@yamaguchi-u.ac.jp.

REFERENCES

1. Fuster V, Badimon L, Badimon J, et al. The pathogenesis of coronary artery disease and the acute coronary syndromes. N Engl J Med 1992;326:242–50, 310–8.
2. Libby P. The molecular basis of the acute coronary syndromes. Circulation 1995;91:2844–50.
3. Yock PG, Johnson EL, Linker DT. Intravascular ultrasound: development and clinical potential. Am J Card Imaging 1988;2:185–93.
4. Gussenhoven EJ, Essed CE, Lancee CT, et al. Arterial wall characteristics determined by intravascular ultrasound imaging: an in vitro study. J Am Coll Cardiol 1989;14:947–52.
5. Tobis JM, Mallery J, Mahon D, et al. Intravascular ultrasound imaging of human coronary arteries in vivo. Analysis of tissue characterizations with comparison to in vitro histological specimens. Circulation 1991; 83:913–26.
6. Mallery JA, Tobis JM, Griffith J, et al. Assessment of normal and atherosclerotic arterial wall thickness with an intravascular ultrasound imaging catheter. Am Heart J 1990;119:1392–400.
7. Nissen SE, Grines CL, Gurley JC, et al. Application of a new phased-array ultrasound imaging catheter in the assessment of vascular dimensions: in vivo comparison to cineangiography. Circulation 1990; 81:660–6.
8. Potkin BN, Bartorelli AL, Gessert JM, et al. Coronary artery imaging with intravascular high-frequency ultrasound. Circulation 1990;81: 1575–85.
9. Nissen SE, Gurley JC, Grines CL, et al. Intravascular ultrasound assessment of lumen size and wall morphology in normal subjects and patients with coronary artery disease. Circulation 1991;84:1087–99.
10. Nishimura RA, Edwards WD, Warnes CA, et al. Intravascular ultrasound imaging: in vitro validation and pathologic correlation. J Am Coll Cardiol 1990;16:145–54.

11. Hodgson JM, Graham SP, Savakus AD, et al. Clinical percutaneous imaging of coronary anatomy using an over-the-wire ultrasound catheter system. Int J Card Imaging 1989;4:187–93.
12. Di Mario C, The SH, Madretsma S, et al. Detection and characterization of vascular lesions by intravascular ultrasound: an in vitro study correlated with histology. J Am Soc Echocardiogr 1992;5:135–46.
13. Friedrich GJ, Moes NY, Muhlberger VA, et al. Detection of intralesional calcium by intracoronary ultrasound depends on the histologic pattern. Am Heart J 1994;128:435–41.
14. Bartorelli AL, Potkin BN, Almagor Y, et al. Plaque characterization of atherosclerotic coronary arteries by intravascular ultrasound. Echocardiography 1990;7:389–95.
15. Peters RJ, Kok WE, Havenith MG, et al. Histopathologic validation of intracoronary ultrasound imaging. J Am Soc Echocardiogr 1994;7: 230–41.
16. Hiro T, Leung CY, Russo RJ, et al. Variability in tissue characterization of atherosclerotic plaque by intravascular ultrasound: a comparison of four intravascular ultrasound systems. Am J Card Imaging 1996; 10:209–18.
17. Hiro T, Leung CY, De Guzman S, et al. Are soft echoes really soft? Intravascular ultrasound assessment of mechanical properties in human atherosclerotic tissue. Am Heart J 1997;133:1–7.
18. Kimura BJ, Bhargava V, DeMaria AN. Value and limitations of intravascular ultrasound imaging in characterizing coronary atherosclerotic plaque. Am Heart J 1995;130:386–96.
19. Jeremias A, Kolz ML, Ikonen TS, et al. Feasibility of in vivo intravascular ultrasound tissue characterization in the detection of early vascular transplant rejection. Circulation 1999;100:2127–30.
20. Bridal SL, Fornes P, Bruneval P, et al. Parametric (integrated backscatter and attenuation) images constructed using backscattered radio frequency signals (25–56 MHz) from human aortae in vitro. Ultrasound Med Biol 1997;23:215–29.
21. Linker DT, Yock PG, Gronningsaether A, et al. Analysis of backscattered ultrasound from normal and diseased arterial wall. Int J Card Imaging 1989;4:177–85.
22. Kawasaki M, Takatsu H, Noda T, et al. Non-invasive tissue characterization of human atherosclerotic lesions in carotid and femoral arteries by ultrasound integrated backscatter: comparison between histology and integrated backscatter images before and after death. J Am Coll Cardiol 2001;38:486–92.
23. Kawasaki M, Takatsu H, Noda T, et al. In vivo quantitative tissue characterization of human coronary arterial plaques by use of integrated backscatter intravascular ultrasound and comparison with angioscopic findings. Circulation 2002;105:2487–92.
24. Wilson LS, Neale ML, Talhami HE, et al. Preliminary results from attenuation-slope mapping of plaque using intravascular ultrasound. Ultrasound Med Biol 1994;20:529–42.
25. Daubechies I, Grossmann A. An integral transform related to quantization. J Mat Phys 1980;21:2080–90.
26. Benkeser PJ, Churchwell AL, Lee C, et al. Resolution limitations in intravascular ultrasound imaging. J Am Soc Echocardiogr 1993;6: 158–65.
27. Nair A, Kuban BD, Tuzcu EM, et al. Coronary plaque classification with intravascular ultrasound radiofrequency data analysis. Circulation 2002;106:2200–6.
28. de Korte CL, Sierevogel MJ, Mastik F, et al. Identification of atherosclerotic plaque components with intravascular ultrasound elastography in vivo: a Yucatan pig study. Circulation 2002;105: 1627–30.
29. Hiro T, Fujii T, Yasumoto K, et al. Detection of fibrous cap in atherosclerotic plaque by intravascular ultrasound by use of color mapping of angle-dependent echo-intensity variation. Circulation 2001;103:1206–11.

Journal of the American College of Cardiology
© 2005 by the American College of Cardiology Foundation
Published by Elsevier Inc.

Vol. 46, No. 8, 2005
ISSN 0735-1097/05/$30.00
doi:10.1016/j.jacc.2005.06.069

Longitudinal Structural Determinants of Atherosclerotic Plaque Vulnerability

A Computational Analysis of Stress Distribution Using Vessel Models and Three-Dimensional Intravascular Ultrasound Imaging

Koji Imoto, MD,* Takafumi Hiro, MD, PHD,* Takashi Fujii, MD, PHD,* Akihiro Murashige, MD, PHD,* Yusaku Fukumoto, MD,* Genta Hashimoto, MD,* Takayuki Okamura, MD, PHD,* Jutaro Yamada, MD, PHD,* Koji Mori, PHD,† Masunori Matsuzaki, MD, PHD, FACC*

Ube, Japan

OBJECTIVES This study theoretically examined the longitudinal structural determinants of plaque vulnerability using a color-coded stress mapping technique for several hypothetical vessel models as well as three-dimensional intravascular ultrasound (IVUS) images with use of a finite element analysis.

BACKGROUND It has been shown that an excessive concentration of stress is related to atherosclerotic plaque rupture. However, the local determinants of in-plaque longitudinal stress distribution along the coronary arterial wall remain unclear.

METHODS Using a finite element analysis, we performed a color mapping of equivalent stress distribution within plaques for three-dimensional vessel models as well as longitudinal IVUS plaque images (n = 15). Then, the effects of plaque size, shape, expansive remodeling, calcification, and lipid core on the equivalent stress distribution were examined.

RESULTS The color mapping of vessel models revealed a concentration of equivalent stress at the top of the hills and the shoulders of homogeneous fibrous plaques. Expansive remodeling and the lipid core augmented the surface equivalent stress, whereas luminal stenosis and superficial calcification attenuated the equivalent stress. The location of excessive stress concentration was modified by the distribution of the lipid core and calcification. The thickness of the fibrous cap was inversely related to the equivalent stress within the fibrous cap. However, the color mapping of IVUS plaque images showed that the equivalent stress value at the fibrous cap varied with changes in plaque shape and superficial calcification, even when the thickness of the fibrous cap remained constant.

CONCLUSIONS A distribution analysis of longitudinal stress revealed specific effects of plaque shape, size, and remodeling, as well as effects of the interior distribution of tissue components, on the concentration of stress at the plaque surface. Moreover, fibrous caps of the same thickness did not consistently represent the same vulnerability to rupture. (J Am Coll Cardiol 2005;46: 1507–15) © 2005 by the American College of Cardiology Foundation

Plaque rupture is a major cause of acute coronary syndrome (1,2). It has been shown that plaque rupture frequently occurs in a noncalcified eccentric atherosclerotic plaque with nonsevere stenosis (3–8), expansive remodeling (9–12), a thin fibrous cap (4,13–17), a large lipid core (4,13–16,18–21), and macrophage infiltration (17,22). Therefore, it is thought that a particular cluster of plaque, referred to as vulnerable plaques, is likely to exist, and the development of a modality for detecting this potentially vulnerable portion in the coronary arterial wall is greatly needed in the clinical setting.

In the process of plaque rupture, an excessive concentration of stress at a certain portion of the plaque surface is considered an important factor (23). An in vitro study reported by Loree et al. (13) showed that thinning of the fibrous cap over a subintimal lipid pool dramatically increased peak circumferential stress in the cross section, especially at the shoulder region of eccentric plaques. However, the local determinants of the distribution of in-plaque longitudinal stress along the coronary arterial wall remain unclear. Therefore, the purpose of this study was to clarify the determinants of the distribution of longitudinal stress within plaques, using a color mapping technique based on computational structural analysis. This color mapping was derived from several hypothetical vessel models as well as from three-dimensional intravascular ultrasound (IVUS) images. The structural computation was performed by a finite element analysis using established material parameters for vessel tissue components (13,19,23,24).

METHODS

Design of vessel models. Initially, various idealized vessel models were designed to examine the effects of plaque morphology and tissue components on longitudinal stress

From the Departments of *Molecular Cardiovascular Biology and †Applied Medical Engineering Science, Yamaguchi University Graduate School of Medicine, Yamaguchi, Ube, Japan. This study was partly supported by a grant-in-aid for scientific research of the Ministry of Education, Japan (grant No. (C)(2)14570666), Health and Labour Sciences Research Grants: Comprehensive Research on Cardiovascular Diseases from Ministry of Health, Labour, and Welfare of Japan, and Knowledge Cluster Initiative of the Ministry of Education, Japan. The first two authors contributed equally to this work. This study was presented in part at the 77th scientific sessions of the American Heart Association, New Orleans, Louisiana, 2004.

Manuscript received February 6, 2005; revised manuscript received June 10, 2005, accepted June 14, 2005.

JACC Vol. 46, No. 8, 2005
October 18, 2005:1507–15

Abbreviations and Acronyms

E = Young moduli
G = shear modulus
IVUS = intravascular ultrasound
P = Poisson ratios

distribution inside the plaque. As shown in Figure 1, a cylindrical vessel model was used, in which an atherosclerotic plaque was formed by the revolution of the same longitudinal sectional structure, thereby avoiding the influence of cross-sectional geometrical factors. This cylindrical model had an inner radius of 1.7 mm and a vessel wall thickness of 0.5 mm at the reference site. In the computational simulation, various plaque morphologies were hypothesized with various stenosis severities and types of vessel remodeling. It was assumed that the plaque components consisted of collagen fibers, calcifications, homogenous lipid tissue, and smooth muscle cells. The blood pressure was considered to be uniform along the vessel walls. The effect of blood flow was neglected in this study. There were no structural limitations in terms of the degree of outward expansion.

As in previous established studies (13,23), all of the components of the atherosclerotic plaques were considered to be orthotropic materials with linear elastic properties. In this study, arteries and fibers provided similar material properties in the circumferential (θ) direction, as well as in the axial (z) direction, which differed from those in the radial (r) direction. Each parameter for the material properties defined in this study is shown in Table 1. In Table 1, E_r and E_θ are the Young moduli in the radial and circumferential directions, respectively. $G_{r\theta}$ is the shear modulus in the $r\theta$ plane, where G_{ij} is the ratio of the shear stress to the shear strain in the ij plane. $P_{r\theta}$ and $P_{\theta z}$ are the Poisson ratios in the $r\theta$ and θz planes, respectively. All of these values have been accepted as the representative values of the material properties of atherosclerotic lesions (13,23). It was assumed that lipids and calcifications were nearly incompressible because of their isotropic properties (23). The Young modulus of lipids was estimated to be 1/100th of the circumferential modulus of a normal artery. The Young modulus of calcified plaques was estimated as 10 times that of the plaque E_θ (13).

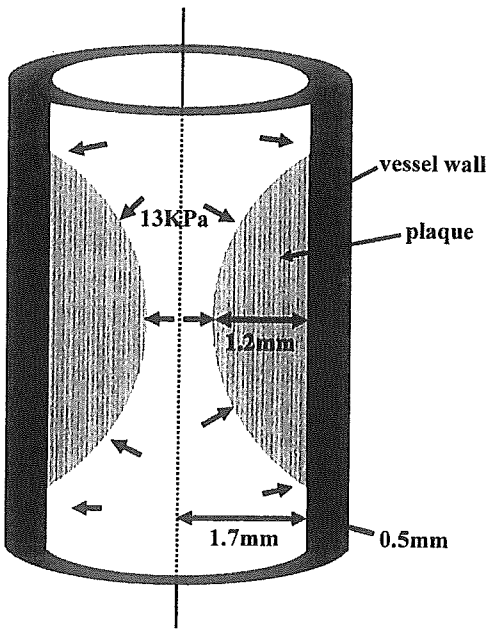

Figure 1. Three-dimensional model. In this vessel model, vessel diameter may vary when a remodeling model is considered.

Structural analysis. The computational structural analysis was performed with a finite element model using a commercially available application (ANSYS 6.0 software, ANSYS Inc., Pittsburgh, Pennsylvania). A complex structure of a vessel model was first divided into smaller subunits designated as elements. The total number of the subunits was approximately 10,000, with a spatial resolution of approximately 100 (10 μm × 10 μm) μm^2. Then, the equivalent stress for each element was calculated. The equivalent stress represented all types of stress for a certain area analyzed, which was calculated from three principal stresses. The structure was automatically meshed with eight-noded quadrilateral plane-strain elements. Each mesh was modified by using an adaptive remeshing algorithm, which was installed in the program. An internal luminal static pressure of 13 kPa (100 mm Hg) was applied along the luminal wall, representing the mean physiological blood pressure in the coronary arteries. Finally, contour plots of equivalent stress were shown on a post-graphics terminal. These contour plots provided two types of colorized mapping, with color codes superimposed on the original structure. One type of mapping was absolute mapping, in which each color code represented a certain range of the absolute value of the equivalent stress; the other type of mapping was relative mapping, in which the color coding was performed by equal division of the range of stress between the maximum and minimum values. According to the computer algorithm, the resulted deformation, such as indentation at the soft part or outward bulging of the normal wall without plaques, was also illustrated.

This study first analyzed the longitudinal stress distribution within plaques for several vessel models with varying structural characteristics of plaque, such as plaque size, plaque shape, stenosis severity, remodeling type, lipid core size, fibrous cap thickness, location and degree of calcification, and so on.

IVUS study. The present study also examined the longitudinal stress distribution in plaques, the structure of which was obtained from the three-dimensional IVUS images. Fifteen human ruptured coronary lesions selected from patients diagnosed with acute coronary syndrome were imaged by IVUS (Atlantis SR pro, 2.8-F, 40-MHz, Boston Scientific Corp./SCIMED, Maple Grove, Minnesota). The transducer was withdrawn automatically using a motorized pullback device (pullback speed, 0.5 mm/s). The IVUS images were all recorded on S-VHS videotape for off-line

Table 1. Material Parameters for Arteries, Plaques, Calcifications, and Lipids Used in Finite Element Models

	Young Moduli (E)			Poisson Ratios (P)			Shear Moduli (G)		
	r	θ	z	rθ	θz	zr	rθ	θz	zr
Artery	10	100	10	0.01	0.27	0.27	50	50	50
Plaque	50	1000	50	0.01	0.27	0.27	500	500	500
Calcification	10,000	10,000	10,000	0.48	0.48	0.48			
Lipid	1	1	1	0.48	0.48	0.48			

r, θ, and z = radial, circumferential, and axial directions, respectively.

analysis. The images were then digitized and analyzed with commercially available software for longitudinal reconstructive IVUS image analysis (Netra IVUS, ScImage Inc., Los Altos, California).

The rupture was defined by an apparent morphology in IVUS images along with comparable clinical history, electrocardiograms, and echocardiograms. No definitive thrombus was detected around the plaque both in IVUS and in angiography. Ruptured plaques with a distinct cavity as well as a significant residual fibrous flap were selected to predict surface morphology before rupture by extrapolating the line of lumen-intima interface.

It was assumed that the ulceration cavity detected by IVUS used to be a lipid core, and that a fibrous cap of a certain thickness used to cover the lipid core. In this in vivo analysis, it was also presumed that the arteries and the plaque components had orthotropic linearly elastic material properties, and that the plaques consisted of homogeneous

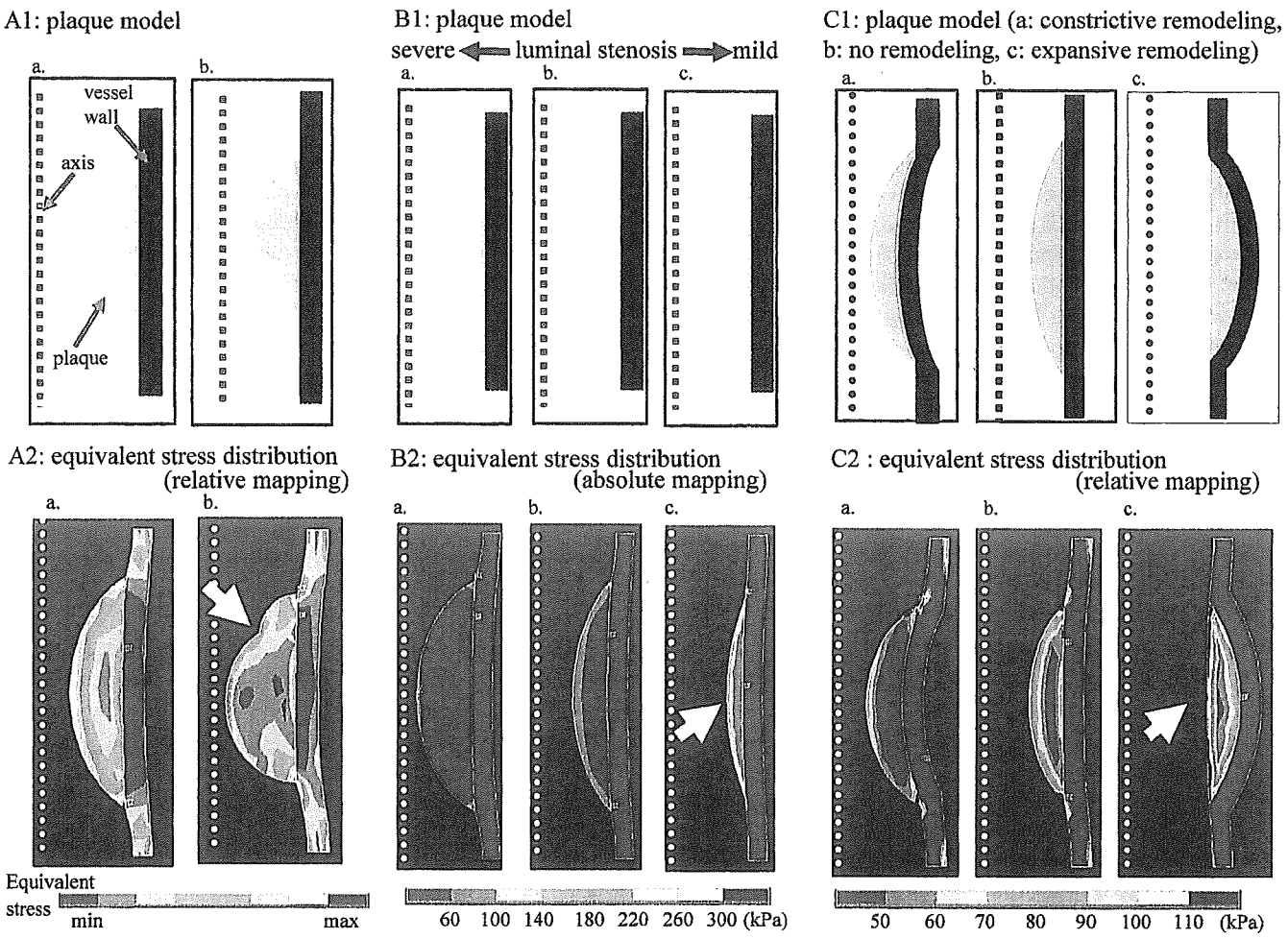

Figure 2. Relationship between stress distribution and plaque shape, luminal stenosis, or vessel remodeling. **(A1, A2)** Color mapping of longitudinal stress distribution within a homogeneous hill-like fibrous plaque model and a complex-shaped model. Relative mapping **(A2)** was performed in the automatically determined window between the maximum and minimum value of stress. The **arrows** designate the sites of stress concentration. **(B1, B2)** Relationship between luminal stenosis and stress distribution. Absolute mapping **(B2)** represents the distribution of the absolute value of equivalent stress. There was a negative relationship between the equivalent stress and luminal stenosis. **(C1, C2)** Relationship between vessel remodeling and stress distribution. The equivalent stress at the plaque surface of arteries with expansive remodeling was greater than that of arteries with constrictive remodeling, when the plaque thickness remained constant.

fibrous tissue, with the exception of the ulcerous cavities and calcifications. However, the original thickness of the fibrous cap of ruptured plaques was unknown. Therefore, in this study, fibrous caps with various thicknesses were considered for the same plaque. Previous in vitro study (19) of human atherosclerotic materials has shown that fibrous caps usually fracture when the static stress exceeds 300 kPa. Therefore, the critical value for fibrous cap thickness, under which the stress on the fibrous cap would exceed 300 kPa, was also calculated for each plaque. This critical thickness was obtained with the abovementioned computer simulation of finite element models. When the critical fibrous cap is thin, it means that the plaque therefore seemed to be less vulnerable. The data were then used to conduct a computational stress analysis using the finite element model for the purpose of color mapping the longitudinal stress distribution, which was superimposed onto the original IVUS images.

This study was approved by the Institutional Review Board of the Hospital of Yamaguchi University School of Medicine. All patients provided signed informed consent to participate in the study before IVUS was performed.

RESULTS

Study of vessel models. This study showed the longitudinal stress distribution within plaques using a color-coded representation. Figure 2A illustrates the longitudinal distribution of equivalent stress within a hill-like homogeneous plaque model by use of relative color mapping. The concentration of equivalent stress could be observed at the top of the plaque hills, as well as at its shoulders. When there was a distortion of plaque shape, the stress was concentrated not only at the summits and shoulders, but also at dips in the irregular surfaces of plaque hills. There was a negative relationship between equivalent stress and luminal stenosis (Fig. 2B). When there was a remodeling of the vascular diameter at a constant maximum plaque thickness, the equivalent stress at the plaque surface of arteries with expansive remodeling was greater than that of arteries with constrictive remodeling (Fig. 2C).

When there was a lipid core, the stress was particularly concentrated at a localized surface area just above the lipid core (Fig. 3). The size of the lipid core had no influence on the surface stress value, given that the thickness of the fibrous cap

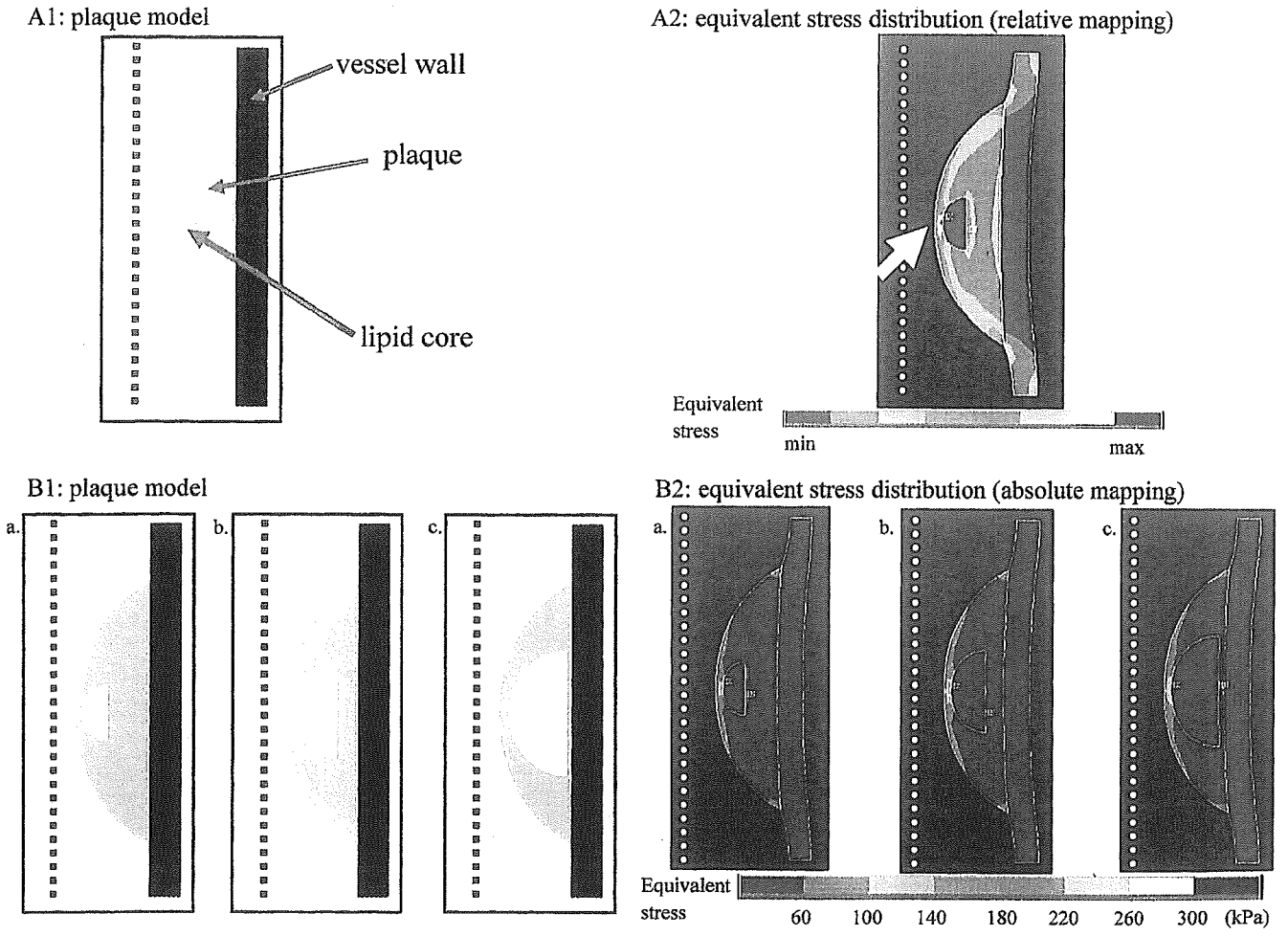

Figure 3. Effect of lipid core on stress distribution. The **arrow** indicates the point of stress concentration at a localized surface area just above the lipid core **(A2)**. The size of the lipid core did not influence the value of the surface stress **(B2)**, provided the fibrous cap thickness remained constant. **(A1, B1)** Plaque models used. **(A2, B2)** Mapping of stress distribution of the corresponded model.

remained constant. However, the thickness of the fibrous cap exerted a great impact on the surface equivalent stress of the plaque, namely, the thinner the fibrous cap, the greater the surface equivalent stress, given that the size of the lipid core remained constant (Fig. 4). In this idealized model, the peak equivalent stress reached beyond the empirical critical level leading to plaque rupture, when the fibrous cap was thinner than 80 μm. Superficial calcifications led to a decrease in surface stress, whereas calcification at the bottom of the plaque exerted no influence on the surface equivalent stress value. As in Figure 5, a superficial calcification adjacent to the lipid core attenuated the peak stress value at the plaque surface just above the lipid core. There was an inverse relationship between the surface equivalent stress and the thickness of the fibrous cap. The stress value increased dramatically when the fibrous cap was thinner than 80 μm. However, when there was a surface calcification near the lipid core, the surface equivalent stress was smaller with the same fibrous cap thickness, such that the inverse relationship shifted leftward and downward (Fig. 6).

IVUS study. Figure 7 shows representative examples of the color mapping of longitudinal stress distribution using longitudinal IVUS images. In case 1, the critical thickness of the fibrous cap leading to rupture was 50 μm, whereas this value was 10 μm in case 2. In case 2, there was a superficial calcification close to the rupture point. Table 2 shows the profile of the 15 ruptured plaques analyzed. The IVUS study showed that the critical thickness of fibrous caps leading to rupture varied between <10 μm and 200 μm.

DISCUSSION

This study was the first showing the longitudinal structural determinants of plaque vulnerability by use of a simplified computational analysis of stress distribution within atherosclerotic plaques using vessel models and three-dimensional intravascular ultrasound imaging. Furthermore, this study also showed that the critical thickness of fibrous caps leading to rupture varied substantially with differences in plaque structure, especially with differences in the degree of calcification.

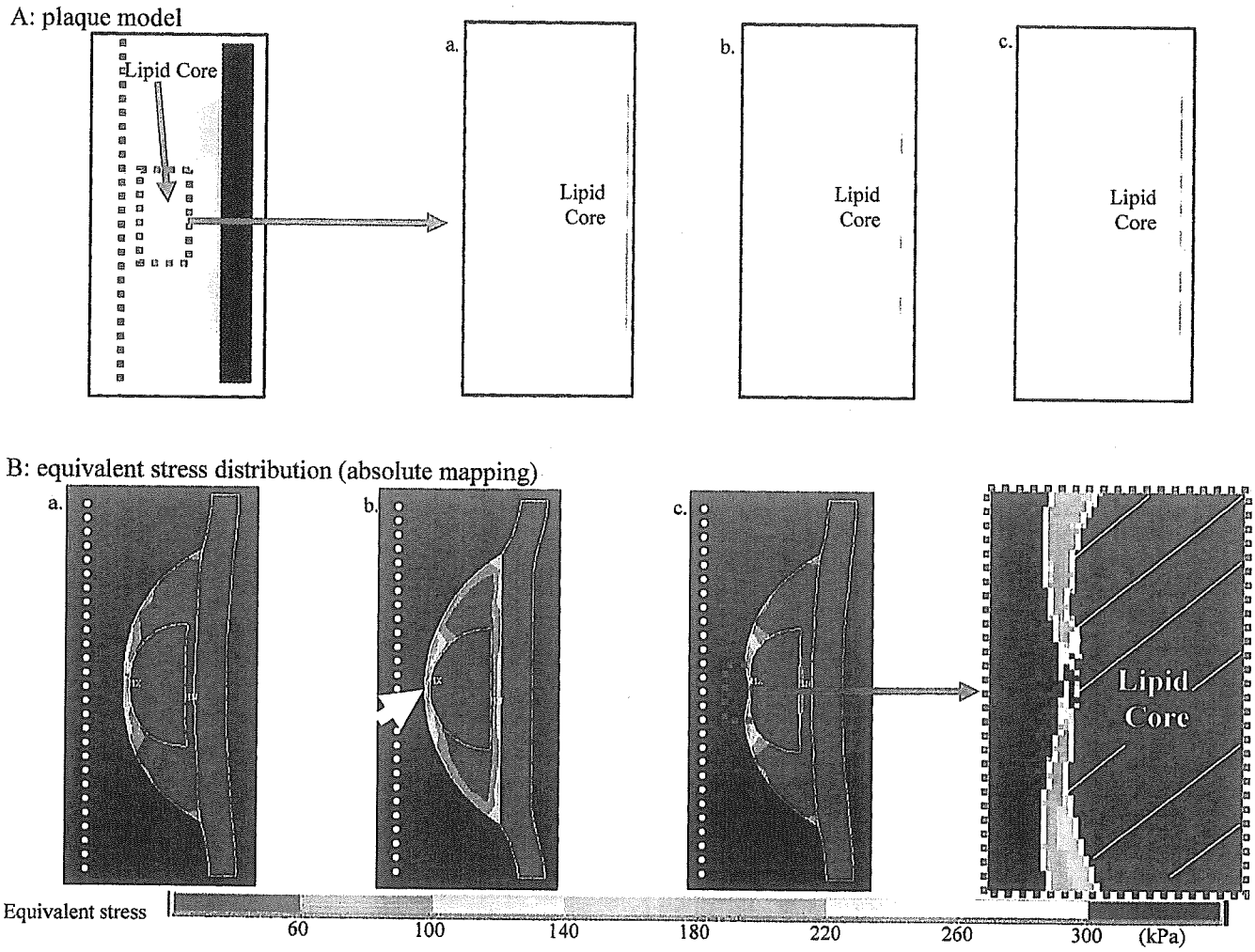

Figure 4. Effect of fibrous cap thickness (**a,** 90 μm; **b,** 80 μm; **c,** 40 μm) on stress distribution. When the fibrous cap was thinner than 80 μm, the stress was markedly elevated **(arrow). (Aa, Ab, Ac)** Plaque models used. **(Ba, Bb, Bc)** Mapping of stress distribution of the corresponded model.

JACC Vol. 46, No. 8, 2005
October 18, 2005:1507–15

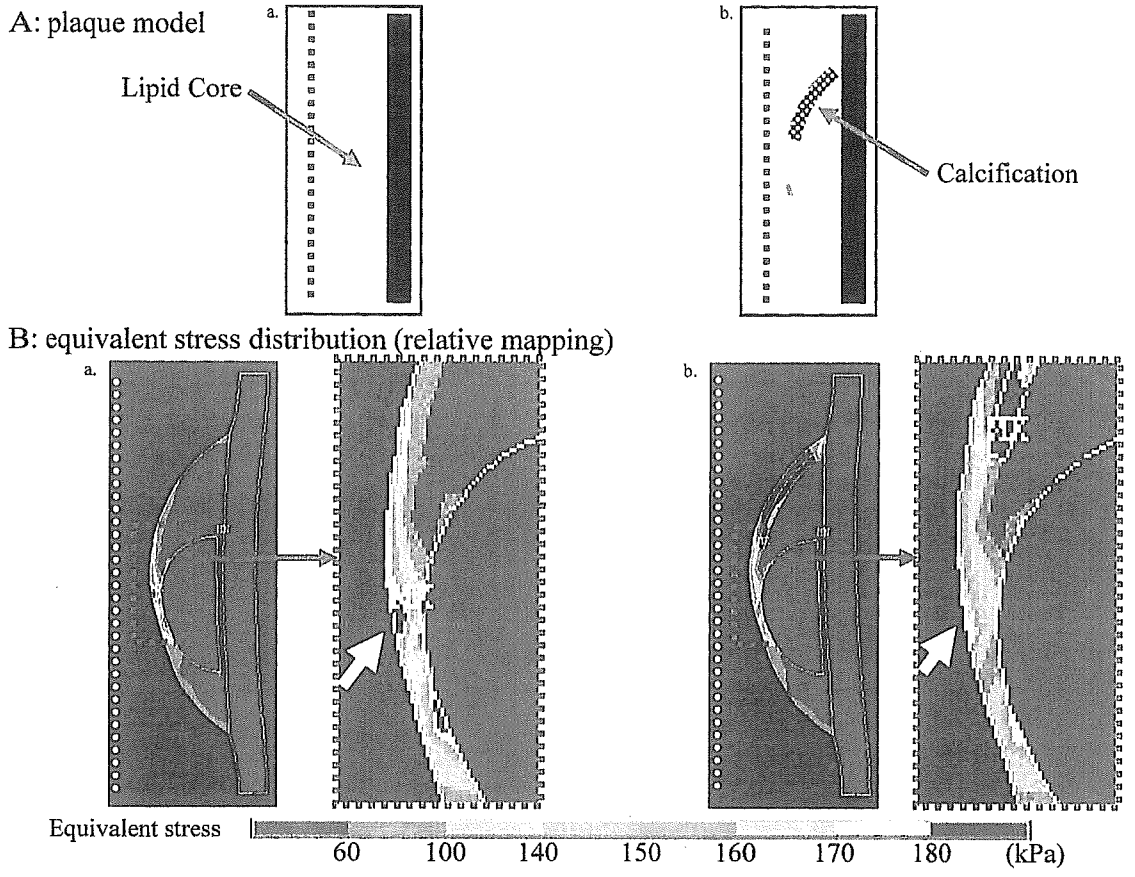

Figure 5. The effect of surface calcifications on the distribution of stress in the surrounding tissue. The size and the place of the lipid core remained constant. A superficial calcification adjacent to the lipid core attenuated the peak stress value at the plaque surface just above the lipid core **(arrow)**. **(Aa, Ab)** Plaque models used. **(Ba, Bb)** Mapping of stress distribution of the corresponded model.

Plaque size, shape, vessel remodeling, and plaque stress. Previous cross-sectional structural analyses of plaque stress distribution have shown that the shoulder regions of eccentric plaques are likely to exhibit stress concentration, leading to a susceptibility to rupture (13). However, the results of this study indicated that longitudinal plaque shape is also important for predicting the location of stress concentration within plaques.

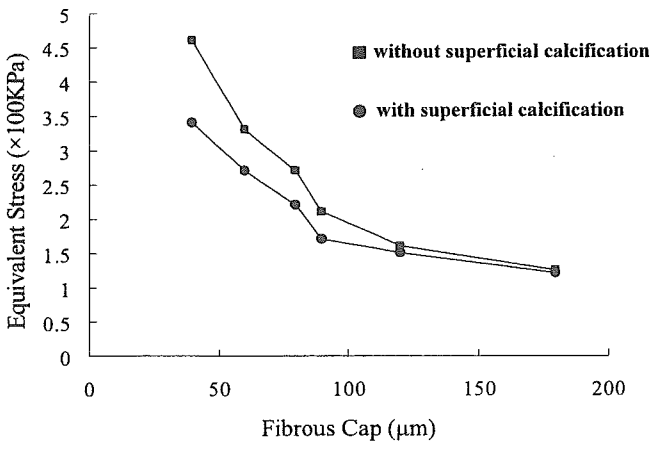

Figure 6. Effect of superficial calcifications on the relationship between the fibrous cap thickness and the peak equivalent stress at the plaque surface. The equivalent stress increased dramatically when the fibrous cap thickness became <80 μm. This increase shifted leftward and downward when there was a superficial calcification close to the area of interest.

Our study showed that increasing either plaque volume or the severity of stenosis decreased the degree of stress concentration. These findings were compatible with those of a previous cross-sectional structural analysis of plaques (13). According to the LaPlace law, the tensile stress on the wall of a luminal structure is correlated with luminal pressure and diameter, and is inversely related to the thickness of the wall. Increasing plaque volume thus increases the thickness of a wall and decreases the luminal diameter (unless there is vessel remodeling), thereby leading to a decrease in the surface stress of the plaque. The present results may therefore account for previous serial angiographic analyses showing that the culprit lesion before the acute event frequently had <50% diameter stenosis (3–8). Based on recent IVUS studies, it is likely that plaque regression or less progression that may not lead to stress attenuation is associated with a decrease in the risk of future cardiac events (9–11). Therefore, this paradoxical consequence could be attributed to simultaneous changes in plaque composition and fibrous cap thickness.

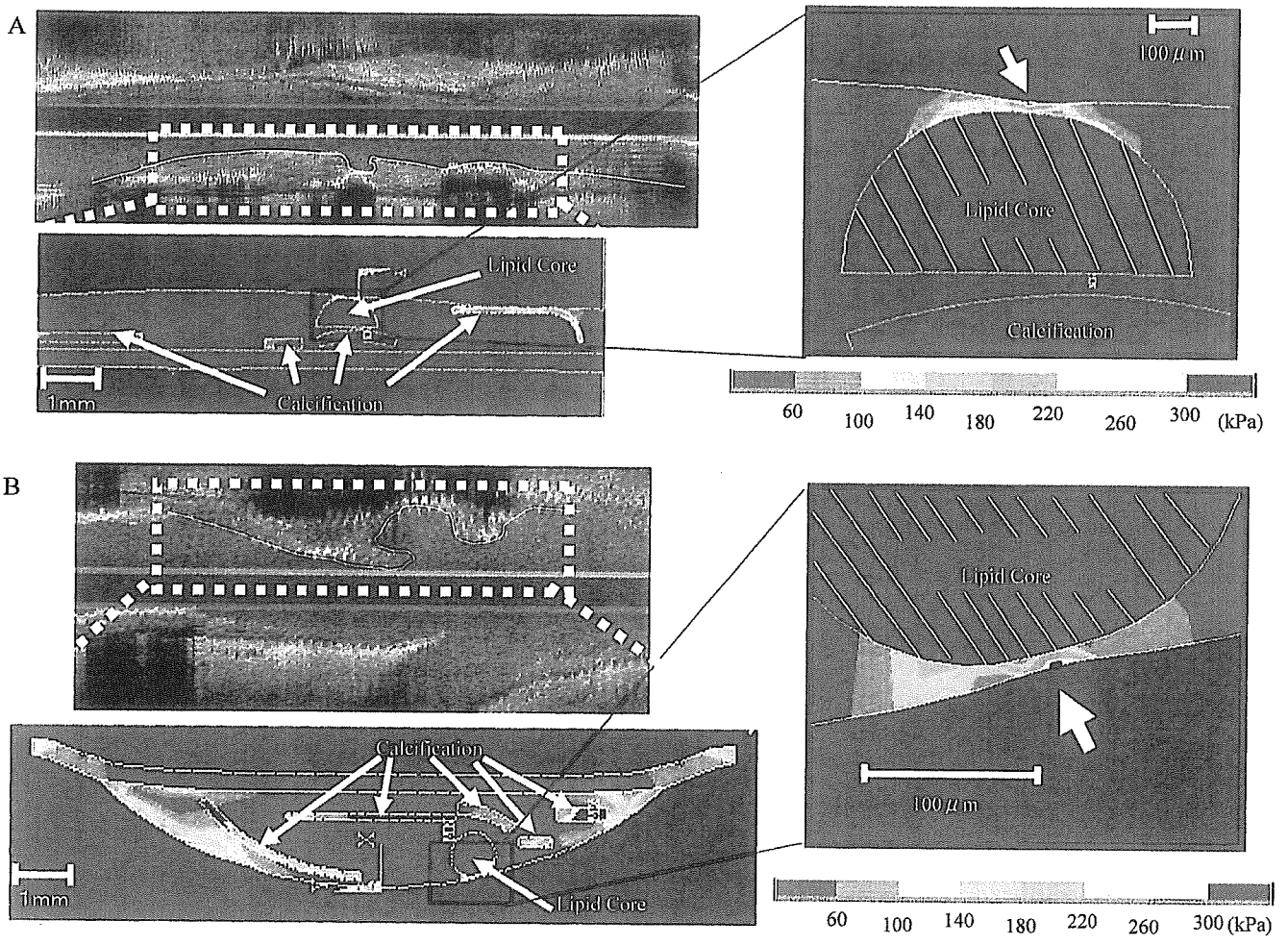

Figure 7. Representative examples of the three-dimensional IVUS images and the color mappings of longitudinal stress distribution. The **arrows** show rupture points. In case 1, the critical thickness of the fibrous cap in terms of rupture was 50 μm **(A)**. However, the thickness in case 2 had to be reduced to <10 μm to reach the critical point in terms of plaque rupture **(B)**. Thus, case 2 seemed to represent a less vulnerable plaque than case 1, although the fibrous cap thickness was the same. **(A)** Case 1; **(B)** case 2.

Table 2. Ruptured Plaque Characteristics Detected by IVUS and Its Simulated Critical Fibrous Cap Thickness

Case	Coronary Artery	Longitudinal Plaque Length	Plaque Thickness	Vessel Diameter	Ulcer Diameter	Superficial Ca	D (mm)	Deep Ca	Critical Fibrous Cap Thickness (μm)
1	LAD	14.6	2.6	5.2	3.1	+	0.8	+	<1
2	RCA	21.0	1.9	4.1	3.2	+	0	+	40
3	LAD	40.0	1.7	4.6	1.8	+	2.4	+	50
4	LAD	12.3	1.2	4.9	2.1	−	−	−	200
5	RCA	26.4	2.0	4.1	0.8	−	−	+	<10
6	LAD	13.2	2.1	5.1	1.7	+	0.7	+	20
7	LAD	5.9	1.2	4.0	0.9	+	2.0	+	15
8	LAD	5.3	1.4	3.6	0.7	−	−	+	60
9	LAD	5.1	1.3	3.3	0.8	−	−	+	60
10	LAD	15.5	2.6	4.0	1.5	−	−	+	<10
11	LAD	12.0	2.1	3.9	1.0	−	−	−	<10
12	LAD	8.2	2.1	3.5	1.8	−	−	+	<10
13	LAD	10.6	1.3	2.9	1.7	−	−	−	20
14	LAD	11.0	1.5	5.2	1.2	+	1.2	+	140
15	LAD	11.3	1.7	3.3	0.6	−	−	+	<10

Ca = calcification; D = distance between edge of superficial calcification and orifice of ulceration; IVUS = intravascular ultrasound; LAD = left anterior descending artery; RCA = right coronary artery.

In this study, when the plaque thickness remained constant, expansive remodeling led to a greater concentration of stress than did constrictive remodeling. Expansive remodeling is frequently observed as a compensatory process for an increase in plaque thickness. In such a case, stress attenuation by the increase in plaque thickness is canceled by expansion in vessel diameter, which consequently maintains or enhances stress value on the plaque surface. Therefore, the present results may be consistent with the findings of previous reports (9–12) showing that unstable plaques are usually associated with expansive remodeling.

Subintimal plaque structure and stress. The significant impact of decreases in fibrous cap thickness on stress concentration within plaques has been widely shown in various studies using postmortem pathological analyses and intravascular imaging modalities (4,13–17). Our findings showed that the stress on a fibrous cap was dramatically increased when its thickness was <80 μm. This value of 80 μm actually depends on the vessel diameter. The range of cap thickness of 60 to 100 μm corresponds to vessel diameters of 2.5 to 4mm. Previous empirical cross-sectional studies have shown that a fibrous cap thickness of less than 65 to 150 μm is critical in terms of the risk of plaque rupture (15,16,25–27). Therefore, the critical thickness of fibrous caps in terms of plaque rupture might be similar in both the cross-sectional and the longitudinal direction. However, the present study using longitudinal IVUS showed that the critical thickness of a fibrous cap leading to rupture varies greatly because of differences in the distribution of surrounding calcifications, even with the same vessel diameter. The involvement of calcification, and variabilities in plaque thickness and shape, may account for inconsistencies regarding the critical thickness reported in several previous studies, which has been shown to vary between 65 and 150 μm (15,16,25–27). The effect of vessel size would also account for a range of the critical thickness varying from 60 to 100 μm as noted above. Furthermore, our results suggest that the measurement of fibrous cap thickness alone is inadequate for identifying plaques vulnerable to rupture.

The presence of a lipid core was also an important factor in stress concentration, according to our study of the longitudinal vessel axis. However, increasing the size of a lipid core did not affect the surface stress of plaques, provided the thickness of the fibrous cap remained constant. These studies, as well as our own, may support the findings of previous reports showing that plaque rupture can be observed in the region of a fibrous cap, even in the presence of a very small lipid core (18,25,28).

Calcification is commonly found in atherosclerosis, but the role of calcification in plaque rupture is still unknown. Some studies indicate beneficial effects in stabilizing plaque (19,23,29), whereas some suggest its worsening effects to plaque vulnerability (30–34). In our study, calcification significantly affected the stress on fibrous caps that were either adjacent to or at a slight distance from calcifications. The exact mechanisms of the attenuation of stress by surface calcification are unclear.

Clinical implications. Although a variety of factors may participate in the process of plaque rupture, including hemodynamic shear stress (20), turbulent pressure fluctuations (35), transient compression (36), sudden increase in intraluminal pressure (37), rupture of the vaso vasorum (38), material fatigue (4,18,39), and cellular inflammatory reactions (3,4,22,40), this study suggests that assessment of stress concentration within a plaque along the longitudinal axis of a vessel is also important for identifying vulnerable plaques. Therefore, this approach may help identify vulnerable plaques or even help predict the point of future rupture.

Study limitations. To simplify the present finite element analysis, the materials were assumed to be isotropic, incompressible, and uniform solids. By assuming that plaques, lipids, calcium, and normal arterial walls could each be characterized by a single set of structural parameters, spatial and interspecimen variations within a particular component were not considered here. However, the assumptions used in this study have been widely accepted as allowable for the assessment of the biomechanical properties of atherosclerotic lesions (13,23). The model used in this study was a linear one, although almost all of the biomaterials have nonlinear properties. Actually, there are only limited data available with regard to the nonlinear biomechanical behavior of atherosclerotic lesions. Furthermore, in the present study, we examined factors affecting relative stress values and not exact absolute stress magnitudes.

In this study, we used an axisymmetric model, although clinical plaques are not always axisymmetric in geometry. The purpose of this study was limited to assess the longitudinal determinants of plaque vulnerability, but not cross-sectional determinants, which were already clarified in the numerous previous studies. Therefore, the axisymmetric model was used to exclude the cross-sectional determinants of stress distribution within plaques.

It was also assumed in this study that there were no shear stresses, torques, time-varying forces, or flow-related forces; only static blood pressure was considered to be acting on the lesion in the models. It has been documented that the effect of fluid shear stress is insignificant when compared with the effect of tensile wall stresses (19) as a direct component in plaque fracture dynamics. The estimation of stresses induced by static pressure load alone has already shown its usefulness in identifying stress concentration in human lesions (23), because the location of stress concentration does not significantly differ between the single static pressure model and the complex dynamic pressure model.

Reprint requests and correspondence: Dr. Takafumi Hiro, Department of Molecular Cardiovascular Biology, Yamaguchi University Graduate School of Medicine, 1-1-1 Minami Kogushi, Ube, Yamaguchi, 755-8505, Japan. E-mail: thiro@yamaguchi-u.ac.jp.

REFERENCES

1. Levin DC, Fallon JT. Significance of the angiographic morphology of localized coronary stenosis: histopathologic correlations. Circulation 1982;66:316–20.
2. Davies MJ, Thomas A. Thrombosis and acute coronary artery lesions in sudden cardiac ischemic death. N Engl J Med 1984;310:1137–40.
3. Shah PK. Mechanism of plaque vulnerability and rupture. J Am Coll Cardiol 2003;41 Suppl 1:15–22.
4. Falk E, Shah PK, Fuster V. Coronary plaque disruption. Circulation 1995;92:657–71.
5. Nobuyoshi M, Tanaka M, Nosaka H, et al. Progression of coronary atherosclerosis: is coronary spasm related to progression? J Am Coll Cardiol 1991;18:904–10.
6. Giroud D, Li JM, Urban P, Meier B, Rutishauer W. Relation of the site of acute myocardial infarction to the most severe coronary arterial stenosis at prior angiography. Am J Cardiol 1992;69:729–32.
7. Ambrose JA, Tannenbaum MA, Alexopoulos D, et al. Angiographic progression of coronary artery disease and the development of myocardial infarction. J Am Coll Cardiol 1988;12:56–62.
8. Little WC, Constantinescu M, Applegate RJ, et al. Can coronary angiography predict the site of a subsequent myocardial infarction in patients with mild-to-moderate coronary artery disease? Circulation 1988;78:1157–66.
9. Schoenhagen P, Ziada KM, Kapadia SR, Crowe TD, Nissen SE, Tuzcu EM. Extent and direction of arterial remodeling in stable versus unstable coronary syndromes: an intravascular ultrasound study. Circulation 2000;101:598–603.
10. Birgelen CV, Klinkhart W, Mintz GS, et al. Plaque distribution and vascular remodeling of ruptured and nonruptured coronary plaques in the same vessel: an intravascular ultrasound study in vivo. J Am Coll Cardiol 2001;37:1864–70.
11. Shoenhagen P, Ziada KM, Vince DG, Nissen SE, Tuzcu EM. Arterial remodeling and coronary artery disease: the concept of "dilated" versus "obstructive" coronary atherosclerosis. J Am Coll Cardiol 2001;38:297–306.
12. Smits PC, Pasterkamp KR, deJaegere PPT, Feyter PJ, Borst C. Angioscopic complex lesions are predominantly compensatory enlarged. Cardiovasc Res 1999;41:458–64.
13. Loree HM, Kamm RD, Stringfellow RG, Lee RT. Effects of fibrous cap thickness on peak circumferential stress in model atherosclerotic vessels. Circ Res 1992;71:850–8.
14. Nissen SE, Yock P. Intravascular ultrasound: novel pathophysiological insights and current clinical applications. Circulation 2001;103:604–16.
15. Maseri A, Fuster V. Is there a vulnerable plaque? Circulation 2003; 107:2068–71.
16. Virmani R, Kolodgie FD, Burke AP, Farb A, Schwartz SM. Lessons from sudden coronary death: a comprehensive morphological classification scheme for atherosclerotic lesions. Arterioscler Thromb Vasc Biol 2000;20:1262–75.
17. Davies MJ, Richardson PD, Woolf N, et al. Risk of thrombosis in human atherosclerotic plaques: role of extracellular lipid, macrophage, and smooth muscle cell content. Br Heart J 1993;69:377–81.
18. Richardson PD, Davies MJ, Born GV. Influence of plaque configuration and stress distribution on fissuring of coronary atherosclerotic plaques. Lancet 1989;2:941–4.
19. Huang H, Virmani R, Younis H, Burke AP, Kamm RD, Lee RT. The impact of calcification on the biomechanical stability of atherosclerotic plaques. Circulation 2001;103:1051–6.
20. Gertz SD, Roberts WC. Hemodynamic shear force in rupture of coronary arterial atherosclerotic plaques. Am J Cardiol 1990;66: 1368–72.
21. Hodgson JM, Reddy KG, Suneja R, Nair RN, Lesnefsky EJ, Sheehan HM. Intracoronary ultrasound imaging: correlation of plaque morphology with angiography, clinical syndrome and procedural results in patients undergoing coronary angiography. J Am Coll Cardiol 1993;21:35–44.
22. Lendon CL, Davies MJ, Born GV, Richardson PD. Atherosclerotic plaque caps are locally weakened when macrophage density is increased. Atherosclerosis 1991;87:87–90.
23. Cheng GC, Loree HM, Kamm RD, Fishibein MC, Lee RT. Distribution of circumferential stress in ruptured and stable atherosclerotic lesions: a structural analysis with histopathological correlation. Circulation 1993;87:1179–87.
24. Lee RT, Loree HM, Cheng GC, Lieberman EH, Jaramillo N, Schoen FJ. Computational structural analysis based on intravascular ultrasound imaging before in vitro angiography: prediction of plaque fracture locations. J Am Coll Cardiol 1993;21:777–82.
25. Ge J, Chirillo F, Schwedtmann J, et al. Screening of ruptured plaques in patients with coronary artery disease by intravascular ultrasound. Heart 1999;81:621–7.
26. Burke AP, Farb A, Malcom GT, Liang Y, Smialek J, Virmani R. Coronary risk factors and plaque morphology in men with coronary disease who died suddenly. N Engl J Med 1997;336:1276–82.
27. MacNeill BD, Lowe HC, Takano M, Fuster V, Jang IK. Intravascular modalities for detection of vulnerable plaque: current status. Arterioscler Thromb Vasc Biol 2003;23:1333–42.
28. Mann JM, Davies MJ. Vulnerable plaque: relation of characteristics to degree of stenosis in human coronary arteries. Circulation 1996;94: 928–31.
29. Alderman EL, Corley SD, Fisher LD, et al. Five-year angiographic follow-up of factors associated with progression of coronary artery disease in the Coronary Artery Surgery Study (CASS). J Am Coll Cardiol 1993;22:1141–54.
30. Raggi P, Callister TQ, Cooil B, et al. Identification of patients at increased risk of first unheralded acute myocardial infarction by electron-beam computed tomography. Circulation 2000;101:850–5.
31. Arad Y, Spadaro LA, Goodman K, Newstein D, Guerci AD. Prediction of coronary events with electron beam computed tomography. J Am Coll Cardiol 2000;36:1253–60.
32. Taylor AJ, Burke AP, O'Malley PG, et al. A comparison of the Framingham risk index, coronary artery calcification, and culprit morphology in sudden cardiac death. Circulation 2000;101:1243–8.
33. Schmermund A, Erbel R. Unstable coronary plaque and its relation to coronary calcium. Circulation 2001;104:1682–7.
34. Mintz GS, Pichard AD, Popma JJ, et al. Determinants and correlates of target lesion calcium in coronary artery disease: a clinical, angiographic and intravascular ultrasound study. J Am Coll Cardiol 1997; 29:268–74.
35. Loree HM, Kamm RD, Atkinson CM, Lee RT. Turbulent pressure fluctuations on surface of model vascular stenosis. Am J Physiol 1991;261:H644–50.
36. Binns RL, Ku DN. Effect of stenosis on wall motion: a possible mechanism of stroke and transient ischemic attack. Arteriosclerosis 1989;9:842–7.
37. Muller JE, Tofler GH, Stone PH. Circadian variation and triggers of onset of acute cardiovascular disease. Circulation 1989;79:733–43.
38. Barger AC, Beeuwkes R, Lainey LL, Silverman KJ. Hypothesis: vasa vasorum and neovascularization of human coronary arteries. A possible role in the pathophysiology of atherosclerosis. N Engl J Med 1984; 310:175–7.
39. MacIsaac AI, Thomas JD, Topol EJ. Toward the quiescent coronary plaque. J Am Coll Cardiol 1993;22:1228–41.
40. Davies MJ. Stability and instability: two faces of coronary atherosclerosis. Circulation 1996;94:2013–20.

Images in Cardiovascular Medicine

A Potential Complication of Directional Coronary Atherectomy

for In-Stent Restenosis

Yuxin Li, MD
Junko Honye, MD
Tadateru Takayama, MD
Shin-Ichiro Yokoyama, MD
Satoshi Saito, MD

We report the case of a patient who underwent directional coronary atherectomy (DCA) for in-stent restenosis of the left anterior descending coronary artery (LAD). After right femoral arterial access, a 10F guiding catheter was used to pass the in-stent restenotic lesion with a 0.014" guide wire. The DCA was performed with a 7F AtheroCath-GTO® atherectomy catheter* (Guidant Corporation; Temecula, Calif). Intravenous ultrasonography (IVUS) was used to optimize the tissue resection. Multiple circumferential cuts were made at pressures from 10 psi to 30 psi. The atherectomy procedure progressed smoothly at a pressure of 10 psi (10 times) and 20 psi (8 times). However, after the 1st cut at a pressure of 30 psi, the cutter suddenly stopped, and the cutter could not be pushed forward or pulled back. The operator then pulled back the whole DCA system into the guiding catheter. No palpable resistance was encountered upon withdrawing the atherectomy catheter; however, fluoroscopic monitoring revealed that the stent was being avulsed from the coronary artery with the atherectomy catheter. After the DCA catheter had been removed, the previously implanted Multi-Link® stent (Guidant Corp.) was found to be trapped between the cutter and the housing (Fig. 1). The stent was removed from the coronary artery. The final angiogram and IVUS revealed that no coronary perforation or other severe complications of the vessel had occurred (Fig. 2).

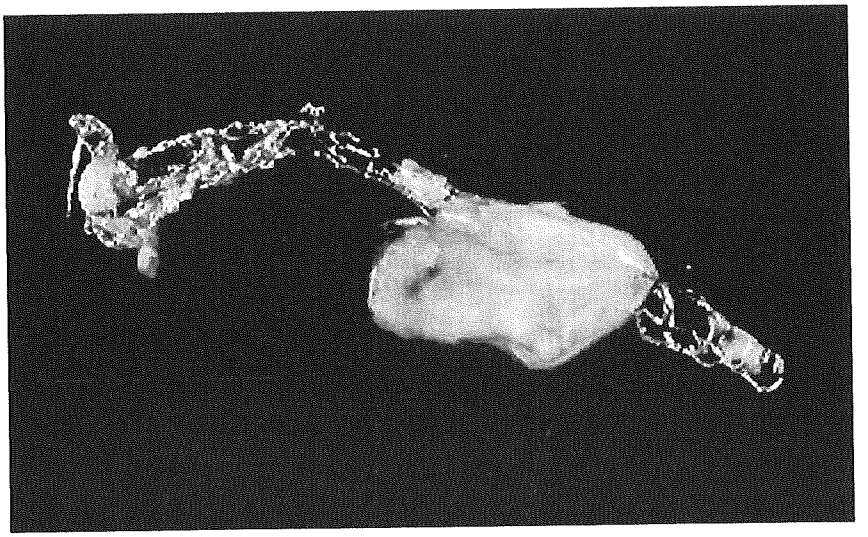

Fig. 1 *Multi-Link® stent (Guidant Corp.) that was pulled out with the whole directional coronary atherectomy catheter system. It is distorted with slight breakage. Part of the plaque and neointima were also pulled out with the stent.*

*This product was placed on the FDA recall list in June 2001 because of dislodgment of the catheter tip in a patient.

Section Editor:
Raymond F. Stainback, MD, Department of Adult Cardiology, Texas Heart Institute and St. Luke's Episcopal Hospital, 6624 Fannin Street, Suite 2480, Houston, TX 77030

From: *Division of Cardiology, the Second Department of Medicine, Nihon University School of Medicine, Tokyo, Japan 173-8610*

Address for reprints:
Satoshi Saito, MD, Division of Cardiology, the Second Department of Medicine, Nihon University School of Medicine, 30-1 Oyaguchi-Kami-machi, Itabashi-ku, Tokyo, Japan 173-8610

E-mail:
Satoshis@med.nihon-u.ac.jp

Discussion

Since approximately 1 million coronary stents are implanted worldwide every year,[1] the management of in-stent restenosis has become a significant challenge for interventional cardiologists. Tissue proliferation is the major cause of in-stent restenosis; therefore, a debulking technique such as directional coronary atherectomy (DCA) would seem to offer a therapeutic advantage by removing the neointimal tissue. Some studies have confirmed the efficacy of DCA for the treatment of in-stent restenosis.[1-3]

The safety of DCA procedures may be dependent on the stent design and construction. Success with DCA has been reported in patients with slotted tube[4] and Palmaz-Schatz[1] stent restenosis. However, implanted stent and vessel disruption have been reported after the use of DCA for the treatment of in-stent restenosis of coil stents.[5,6] In 1 series,[7] 2 out of 50 patients had stents that were apparently deformed by the atherectomy procedure. There were also some small complications or technical difficulties such as the atherectomy devices' becoming blocked several times at higher balloon pressures.[7] In our patient, the previously implanted stent was entrapped and was pulled from the coronary artery. On the basis of our case and previous reports, cardiologists should bear in mind that it is possible for struts to block the cutter. When DCA is used for in-stent restenosis, aiming for optimal debulking may lead to this rare complication. Therefore, a conservative debulking strategy might be safer.

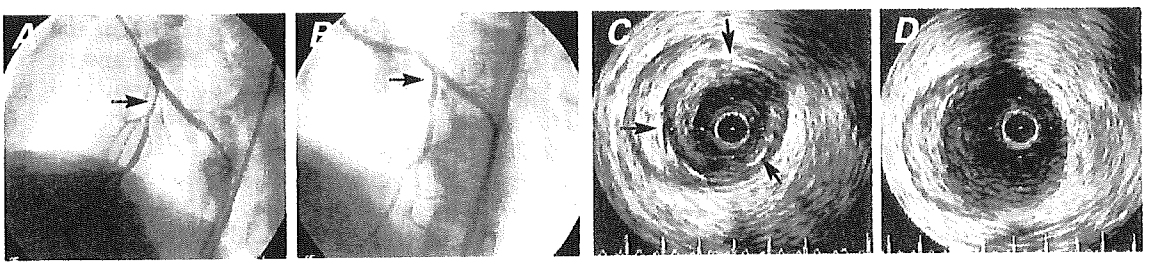

Fig. 2 *Angiograms and intravascular ultrasonographic (IVUS) images of in-stent restenosis before and after directional coronary atherectomy (DCA).* ***A)*** *Angiogram shows 90% diffuse in-stent restenosis in the left anterior descending coronary artery segment 6 (arrow).* ***B)*** *The restenosis is abolished after DCA (as shown by arrow).* ***C)*** *Before DCA, IVUS shows the stent (arrows) and severe neointimal proliferation within the stent.* ***D)*** *The enlarged lumen is shown after DCA, when the stent and neointima were pulled out.*

References

1. Mahdi NA, Pathan AZ, Harrell L, Leon MN, Lopez J, Butte A, et al. Directional coronary atherectomy for the treatment of Palmaz-Schatz in-stent restenosis. Am J Cardiol 1998;82:1345-51.
2. Mintz GS, Hoffmann R, Mehran R, Pichard AD, Kent KM, Satler LF, et al. In-stent restenosis: the Washington Hospital Center experience. Am J Cardiol 1998;81(7A):7E-13E.
3. Dauerman HL, Baim DS, Cutlip DE, Sparano AM, Gibson CM, Kuntz RE, et al. Mechanical debulking versus balloon angioplasty for the treatment of diffuse in-stent restenosis. Am J Cardiol 1998;82:277-84.
4. Palacios IF, Sanchez PL, Mahdi NA. The place of directional coronary atherectomy for the treatment of in-stent restenosis. Semin Interv Cardiol 2000;5:209-16.
5. Macander PJ, Roubin GS, Agrawal SK, Cannon AD, Dean LS, Baxley WA. Balloon angioplasty for treatment of in-stent restenosis: feasibility, safety, and efficacy. Cathet Cardiovasc Diagn 1994;32:125-31.
6. Bowerman RE, Pinkerton CA, Kirk B, Waller BF. Disruption of a coronary stent during atherectomy for restenosis. Cathet Cardiovasc Diagn 1991;24:248-51.
7. Haberbosch W, Waas W, Waldecker B, Heizmann H, Holschermann H, Rau M, Tillmanns H. Directional coronary atherectomy of in-stent restenosis: a two-center experience. J Interv Cardiol 2000;13:93-9.

ELSEVIER

International Journal of Cardiology xx (2005) xxx – xxx

International Journal of Cardiology

www.elsevier.com/locate/ijcard

Letters to the Editor

Whole-heart coronary magnetic resonance angiography in a patient with unstable angina

Yuichi Sato *, Naoya Matsumoto, Shunichi Yoda, Satoshi Kunimoto, Yuji Kasamaki, Tadateru Takayama, Satoru Furuhashi, Motoichiro Takahashi, Takahisa Uchiyama, Satoshi Saito

Department of Cardiology, Nihon University School of Medicine, 1-8-13 Kanda-Surugadai, Chiyoda-ku, Tokyo 101-8309, Japan

Received 22 June 2005; accepted 25 June 2005

Keywords: Whole-heart coronary MR angiography; Unstable angina

1. Case report

A 67-year-old man was transferred to the emergency department because of anterior chest pain which persisted for 30 min. He had no significant coronary risk factors. Upon admission, there were no ST segment elevations or T wave abnormalities. Initial serum creatine kinase was 116 IU/l and troponin I was negative. Echocardiography revealed no left ventricular regional wall motion abnormality. The patient was referred to whole-heart coronary magnetic resonance angiography (MRA) with a provisional diagnosis of unstable angina. MRA was performed using a free-breathing, 3-dimensional navigator technique [1]. Volume rendering image showed stenosis in the proximal portion of the left anterior descending artery (Fig. 1A, arrow). Maximum intensity projection image demonstrated high-grade stenosis in the left anterior descending artery immediately distal to the bifurcation point (Fig. 1B, arrow). Conventional coronary angiography revealed subtotal occlusion of the left anterior descending artery (Fig. 2, arrow).

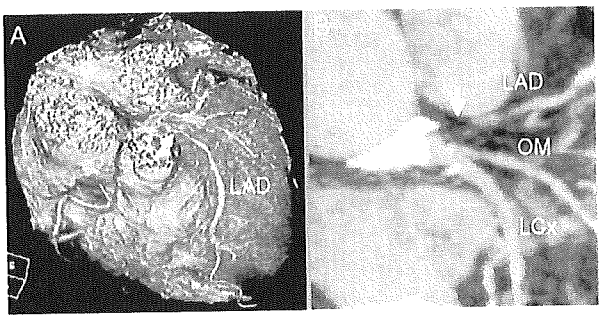

Fig. 1. LAD=left anterior descending artery, LCx=left circumflex artery, and OM=obtuse marginal artery.

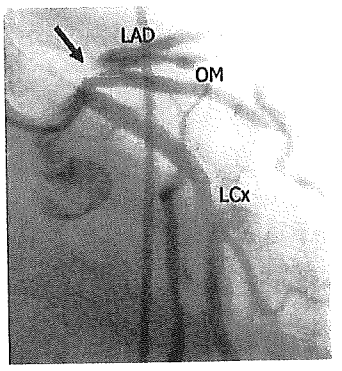

Fig. 2. LAD=left anterior descending artery, LCx=left circumflex artery, and OM=obtuse marginal artery.

2. Discussion

The diagnosis of acute coronary syndrome (ACS) especially non-ST-elevation myocardial infarction and unstable angina in the emergency department still remains a challenge.

* Corresponding author. Tel.: +81 3293 1711; fax: +81 3295 1859.
E-mail address: yuichis@med.nihon-u.ac.jp (Y. Sato).

doi:10.1016/j.ijcard.2005.06.069

Despite the initial risk assessment using ECG and cardiac enzymes, approximately 2% of patients with ACS are inappropriately discharged home from the emergency department [2]. On the other hand, aggressive, invasive procedure is not fully justified because it may expose patients with low likelihood of ACS to angiography-related complications and excessive medical expense. Whole-heart coronary MRA allows totally non-invasive assessment of coronary artery disease and has the potential to become a routine diagnostic tool in patients with suspected ACS in the emergency department.

References

[1] Weber OM, Pujadas S, Martin AJ, Higgins CB. Free-breathing, three-dimensional coronary artery magnetic resonance angiography: comparison of sequences. J Magn Reson Imaging 2004;20:395–402.

[2] Pope JH, Aufdeheide TP, Ruthazer R, et al. Missed diagnosis of acute cardiac ischemia in the emergency department. N Engl J Med 2000; 342:1163–70.